

## GRAVITATIONAL RADIATION FROM NONAXISYMMETRIC SPHERICAL COUETTE FLOW IN A NEUTRON STAR

C. PERALTA,<sup>1,2</sup> A. MELATOS,<sup>1</sup> M. GIACOBELLO,<sup>3</sup> AND A. OOI<sup>3</sup>

Received 2006 March 12; accepted 2006 April 27; published 2006 May 30

### ABSTRACT

The gravitational-wave signal generated by global, nonaxisymmetric shear flows in a neutron star is calculated numerically by integrating the incompressible Navier-Stokes equation in a spherical, differentially rotating shell. At Reynolds numbers  $\text{Re} \geq 3 \times 10^3$  the laminar Stokes flow is unstable, and helical, oscillating Taylor-Görtler vortices develop. The gravitational-wave strain generated by the resulting kinetic energy fluctuations is computed in both plus and cross polarizations as a function of time. It is found that the signal-to-noise ratio for a coherent,  $10^8$  s integration with LIGO II scales as  $6.5[\Omega_*/(10^4 \text{ rad s}^{-1})]^{7/2}$  for a star at 1 kpc with angular velocity  $\Omega_*$ . This should be regarded as a lower limit: it excludes pressure fluctuations, herringbone flows, Stuart vortices, and fully developed turbulence (for  $\text{Re} \geq 10^6$ ).

*Subject headings:* gravitational waves — hydrodynamics — stars: neutron — stars: rotation

### 1. INTRODUCTION

Gravitational radiation from *linear*, global, fluid oscillations in neutron stars has been studied extensively: for example, radiation-reaction-driven  $r$ -modes (Andersson 1998; Levin & Ushomirsky 2001) and two-stream superfluid oscillations with entrainment (Andersson 2003; Prix et al. 2004). However, gravitational radiation is also emitted by *nonlinear*, global, fluid oscillations. Specifically, it is well known that a viscous Navier-Stokes fluid inside a spherical, differentially rotating shell—spherical Couette flow (SCF)—undergoes sudden transitions between states with different vortex topologies, which are generally nonaxisymmetric, due to shear instabilities (Marcus & Tuckerman 1987a, 1987b; Junk & Egbers 2000). Recent simulations of superfluid SCF, based on the Hall-Vinen-Bekarevich-Khalatnikov (HVBK) theory of a  $^1S_0$  neutron superfluid, confirm that such transitions to nonaxisymmetric flows also occur in neutron stars (Peralta et al. 2005, 2006).

In this Letter, we compute the gravitational-wave signal generated by nonaxisymmetric flows in young, rapidly rotating neutron stars. There are at least two astrophysical scenarios in which these develop. First, if the crust and core of the star are loosely coupled, as indicated by observations of pulsar glitches (Shemar & Lyne 1996; Lyne et al. 2000), differential rotation builds up as the crust spins down electromagnetically, until the core undergoes a transition to the Taylor-Görtler vortex state, a helical, oscillating flow that is one of the last stages in the laminar-turbulent transition in SCF as the Reynolds number increases (Nakabayashi 1983; Nakabayashi & Tsuchida 1988). Second, if the crust precesses while the core does not, the rotation axes of the crust and core misalign, inducing a rich variety of flow patterns and instabilities, such as time-dependent shear waves, leading to fully developed turbulence (Wilde & Vanyo 1995). We treat the former scenario here and postpone the latter to a separate paper.

In § 2, an SCF model of a differentially rotating neutron star is proposed. In § 3, we explore the transitional dynamics and topology of the flow. In § 4, we calculate the gravitational-wave signal and its frequency spectrum.

### 2. GLOBAL SCF MODEL AND NUMERICAL METHOD

We consider an idealized, two-component model of a neutron star, in which a solid crust is loosely coupled to a differentially rotating fluid core. Specifically, we consider the motion of a neutron fluid within a spherical, differentially rotating shell in the outer core of the star, where the density  $\rho$  lies in the range  $0.6 < \rho/\rho_c < 1.5$ ,  $\rho_c = 2.6 \times 10^{14} \text{ g cm}^{-3}$  (Sedrakian & Sedrakian 1995). The inner (radius  $R_1$ ) and outer (radius  $R_2$ ) boundaries rotate at angular frequencies  $\Omega_1$  and  $\Omega_2$ , respectively, about the  $z$ -axis. As the star is strongly stratified, the shell is thin, with  $R_2 - R_1 \leq 0.1R_1$  (Abney & Epstein 1996; Levin & D’Angelo 2004). The rotational shear is sustained by the vacuum dipole spin-down torque, violent events at birth (Dimmelmeier et al. 2002; Ott et al. 2004), accretion in a binary (Fujimoto 1993), neutron star mergers (Shibata & Uryū 2000), or internal oscillations such as  $r$ -modes (Rezzolla et al. 2000; Levin & Ushomirsky 2001).

We describe the fluid by the isothermal Navier-Stokes equation, which, in the inertial frame of an external observer, takes the form

$$\frac{\partial \mathbf{v}}{\partial t} + (\mathbf{v} \cdot \nabla) \mathbf{v} = -\frac{\nabla p}{\rho} + \nu \nabla^2 \mathbf{v} + \nabla \Phi \quad (1)$$

in the incompressible limit  $\nabla \cdot \mathbf{v} = 0$ , where  $\mathbf{v}$  is the fluid velocity,  $\nu$  is the kinematic viscosity,  $\rho$  is the density,  $p$  is the pressure, and  $\Phi$  is the Newtonian gravitational potential. Henceforth,  $\Phi$  is absorbed into  $p$  by replacing  $p - \rho\Phi$  with  $p$ , such that pressure balances gravity in the stationary equilibrium ( $\mathbf{v} = 0$ ) and there are no gravitational forces driving the flow in the incompressible limit when the stationary equilibrium is perturbed. The Reynolds number and dimensionless gap width are defined by  $\text{Re} = \Omega_1 R_1^2 / \nu$  and  $\delta = (R_2 - R_1) / R_1$ ; the rotational shear is  $\Delta\Omega = \Omega_2 - \Omega_1$ . Equation (1) is solved subject to no-slip boundary conditions.

Superfluidity plays a central role in the thermal (Yakovlev et al. 1999) and hydrodynamic (Alpar 1978; Reisenegger 1993; Peralta et al. 2005) behavior of neutron star interiors. However, we assume a viscous fluid here. Counterintuitively, this is a good approximation because  $\text{Re} (\sim 10^{11})$  is very high (Mastrano & Melatos 2005). It is known from terrestrial experiments on superfluid  $^4\text{He}$  that, at high  $\text{Re}$ , quantized vortices tend to lock the superfluid to turbulent eddies in the normal fluid by mutual

<sup>1</sup> School of Physics, University of Melbourne, Parkville, VIC 3010, Australia; cperalta@physics.unimelb.edu.au.

<sup>2</sup> Departamento de Física, Escuela de Ciencias, Universidad de Oriente, Cumaná 6101, Estado Sucre, Venezuela.

<sup>3</sup> Department of Mechanical Engineering, University of Melbourne, Parkville, VIC 3010, Australia.

friction (Barenghi et al. 1997), so that the superfluid resembles classical Navier-Stokes turbulence. Moreover, in HVBK simulations of SCF, it is observed that the global circulation pattern of the superfluid does not differ much from a Navier-Stokes fluid at  $\text{Re} \geq 250$  (Henderson & Barenghi 2004; Peralta et al. 2005). Finally, a viscous interior is expected in newly born neutron stars, which are hotter than the superfluidity transition temperature (Andersson et al. 1999).

By assuming a viscous fluid, we omit from equation (1) the coupling between quantized vortices and the normal fluid (Hall & Vinen 1956), entrainment of superfluid neutrons by protons (Comer 2002), and pinning of quantized vortices in the inner crust, at radius  $R_1$  (Baym et al. 1992; cf. Jones 1998). We also neglect vortex pinning in the outer core for simplicity, even though evidence exists that it may be important when magnetic fields are included. Specifically, three-fluid models of postglitch relaxation based on the core dynamics favor vortex pinning at the phase separation boundary of the core (Sedrakian & Sedrakian 1995), for example, due to the interaction between vortex clusters and the Meissner supercurrent set up by the crustal magnetic field at the phase boundary (Sedrakian & Cordes 1999). Other models analyze interpinning of proton and neutron vortices in the core (Ruderman 1991) and its effect on precession (Link 2003). In the context of the hydrodynamic model in this Letter, pinning effectively increases the viscosity of the core, reducing  $\text{Re}$ .

We use a pseudospectral collocation method to solve equation (1) (Bagchi & Balachandar 2002; Giacobello 2005). The equations are spatially discretized in spherical polar coordinates  $(r, \theta, \phi)$ , using restricted Fourier expansions in  $\theta$  and  $\phi$  and a Chebyshev expansion in  $r$ . The solution is advanced using a two-step fractional step method, which is accurate to second order in the time step (Canuto et al. 1988). We limit ourselves to narrow gaps  $\delta \leq 0.1$ , which are computationally less expensive and for which more experimental studies are available for comparison (Yavorskaya et al. 1977; Nakabayashi 1983). Recently, we performed the first stable simulations of superfluid SCF using this method (Peralta et al. 2005).

### 3. NONAXISYMMETRIC SPHERICAL COUETTE FLOW

The bifurcations and instabilities leading to transitions between SCF states are controlled by three parameters:  $\delta$ ,  $\text{Re}$ , and  $\Delta\Omega$ . In addition, the history of the flow influences its post-instability evolution and the final transition to turbulence (Wulf et al. 1999; Junk & Egbers 2000). For example, in experiments on Taylor-Görtler vortices (TGVs), the final state depends on  $d\Omega_1/dt$ , that is, on the time to reach the critical  $\text{Re}$  relative to the viscous diffusion time (Nakabayashi & Tsuchida 1995). In general, four SCF states can be distinguished: (1) a laminar basic flow, (2) a toroidal or helical Taylor-Görtler flow, (3) a transitional flow with nonaxisymmetric, oscillating TGVs, and (4) fully developed turbulence (Yavorskaya et al. 1975; Nakabayashi 1983). In a neutron star, where  $\text{Re} \sim 10^{11}$ , the state is probably turbulent. However, we are restricted by our computational resources to simulate regimes 1 and 2, with  $1 \times 10^3 \leq \text{Re} \leq 3 \times 10^4$ .

#### 3.1. TGV Transition: Initial Conditions

Experimentally, for  $\delta = 0.06$ , TGVs are obtained by quasi-statically increasing  $\Omega_1$  from zero to give  $\text{Re} \sim 3300$  (Nakabayashi & Tsuchida 2005). This procedure can be painfully slow, because a steady state must be reached at each intermediate step. Numerically, we circumvent it by following Li

(2004) and introducing a nonaxisymmetric perturbation with azimuthal wavenumber  $m_a$  of the form

$$v_r = -\frac{4\epsilon_1(r-R_1)(r-R_2)}{\delta^2 R_1^2} \cos \chi(\theta, \phi), \quad (2)$$

$$v_\theta = \frac{\epsilon_1}{\delta} \sin \left[ \frac{\pi(r-R_1)(r-R_2)}{2(R_2-R_1)^2} \right] \sin \chi(\theta, \phi) \quad (3)$$

with  $\chi = \pi[1 - R_2(\frac{1}{2}\pi - \theta)/(R_2 - R_1) - 0.4 \sin m_a \phi]$ . This is done as follows: Before introducing the perturbation, a steady state for  $\text{Re} = 2667$  is obtained (just below the critical  $\text{Re}$  where TGVs emerge experimentally). Then the Reynolds number is raised instantaneously to  $\text{Re} = 3300$ , and we continue by adding equations (2) and (3), with amplitude  $\epsilon_1 \sim 10^{-6} \Omega_1 R_1$ , to the numerical solution at each time step until a viscous diffusion time  $t_d = (R_2 - R_1)^2/\nu$  elapses. We then stop adding the perturbation and the flow is left to evolve according to equation (1) until a final steady state is reached. More than one perturbation can lead to the same final state; some authors add Gaussian noise (Zikanov 1996), although this affords less control over the wavenumber and the number of vortices excited.

The perturbation excites TGVs by shedding vorticity from the inner sphere (Li 2004). Perturbations with  $2 \leq m_a \leq 5$  are explored, supplementing experiments with  $m_a = 3$  (Nakabayashi 1983). For numerical simplicity, we limit ourselves to the case where only the inner sphere rotates. TGVs with both spheres rotating are equally possible and have been observed experimentally; they exhibit additional twisting (and increased nonaxisymmetry) in the helical vortices (Nakabayashi & Tsuchida 2005), so the gravitational-wave strain we compute in § 4 is a lower limit.

#### 3.2. Flow Topology

Figure 1a shows a kinetic energy density isosurface ( $0.11 \times \rho R_1^5 \Omega_1^2$ ) for the fully developed TGV state  $m_a = 3$ ,  $\delta = 0.06$ ,  $\text{Re} = 3300$ . Its nonaxisymmetry is apparent in the striated equatorial bands, whose inclination with respect to the equator varies with longitude from zero to  $\sim 3^\circ$  (Nakabayashi 1983).

A popular way to classify complex, three-dimensional flows is to construct scalar invariants from  $A_{ij} = \partial v_i / \partial x_j$  (Chong et al. 1990; Jeong & Hussain 1995). Specifically, the discriminant  $D_A = Q_A^3 + 27R_A^2/4$ , with  $R_A = -\det(A_{ij})$  and  $Q_A = (A_{ii}^2 - A_{ij}A_{ji})/2$ , distinguishes between regions that are focal ( $D_A > 0$ ) and those that are strain-dominated ( $D_A < 0$ ). Figure 1b plots the  $D_A = 10^{-3} \Omega_1^6$  isosurface in color: yellow regions are stable focus/stretching,<sup>4</sup> and blue regions are unstable focus/contracting. The filaments coincide with the TGVs. One circumferential vortex and  $m_a = 3$  helical vortices lie in each hemisphere. We also plot the isosurface  $D_A = -10^{-3} \Omega_1^6$ : red and green regions have stable-node/saddle/saddle and unstable-node/saddle/saddle topologies, respectively (Chong et al. 1990). The helical vortices span  $\sim 40^\circ$  of latitude and travel in the  $\phi$ -direction, with phase speed  $\approx 0.48 \Omega_1 R_1$ .

The TGV state is oscillatory, which is important for the gravitational-wave spectrum. Its periodicity is evident in Figure 1c, where  $v_\theta$  at an equatorial point is plotted versus time for  $2 \leq m_a \leq 5$ . For  $m_a = 3$ ,  $v_\theta$  oscillates with period  $4.4 \Omega_1^{-1}$ , the time for successive helical vortices to pass by a stationary

<sup>4</sup> Trajectories are repelled away from a fixed point along a real eigenvector of  $A_{ij}$  (stretch) and describe an inward spiral when projected onto the plane normal to the eigenvector (stable focus).

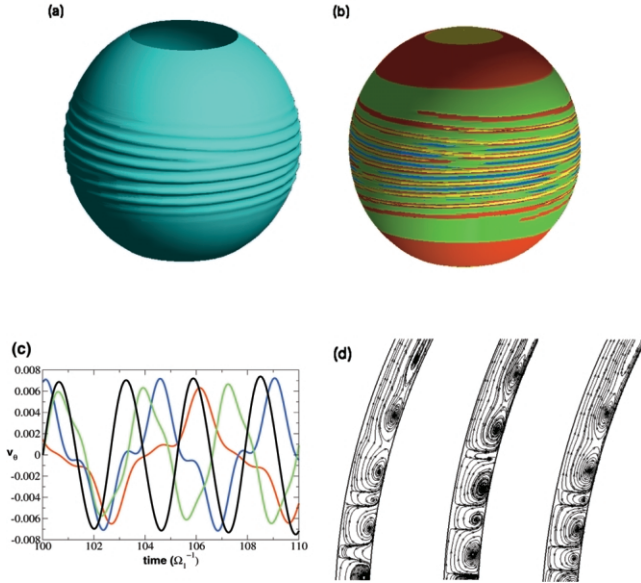


FIG. 1.—Taylor-Görtler vortices for  $m_a = 3$  and  $\delta = 0.06$ , at  $t = 100\Omega_1^{-1}$ . (a) Isosurface of kinetic energy:  $\rho |\mathbf{v}|^2 = 0.11\rho R_1^2\Omega_1^2$ . (b) Isosurfaces of velocity gradient discriminant:  $D_A = 10^{-3}\Omega_1^6$ , stable-focus/stretching (yellow) and unstable-focus/contracting (blue);  $D_A = -10^{-3}\Omega_1^6$ , stable-node/saddle/saddle (red) and unstable-node/saddle/saddle (green). (c) Time history of  $v_\theta$  at  $r = 1.06$ ,  $\theta = \pi/2$ , and  $\phi = 0$  for  $m_a = 2$  (red), 3 (blue), 4 (green), and 5 (black). (d) Streamlines obtained by integrating the in-plane components of  $\mathbf{v}$  in the planes  $\phi = 0$  (left),  $\phi = \pi/2$  (middle), and  $\phi = 2\pi/9$  (right).

observer, in accord with experiments (Nakabayashi 1983). Instantaneous streamlines are drawn in three meridional planes in Figure 1d, highlighting the nonaxisymmetry. One obtains a similar TGV state for  $\delta = 0.14$  and  $\delta = 0.18$  (Sha & Nakabayashi 2001; Li 2004).

#### 4. GRAVITATIONAL-WAVE SIGNAL

The metric perturbation  $h_{ij}^{\text{TT}} = (4G/rc^4) \int d^3\mathbf{x} T_{ij}$  in the transverse-traceless gauge can be calculated using Einstein’s quadrupole formula

$$h_{ij}^{\text{TT}} = \frac{2G\rho}{rc^6} \frac{\partial^2}{\partial t^2} \int d^3\mathbf{x} |\mathbf{v}|^2 \left( x_i x_j - \delta_{ij} \frac{|\mathbf{x}|^2}{3} \right) \quad (4)$$

(Misner et al. 1973), where the integral is over the source volume,  $r$  is the distance to the source, and  $T_{ij} = \rho\gamma^2 v_i v_j + p\delta_{ij}$  is the stress-energy of a Newtonian fluid. Note that we approximate  $T_{00} = \rho\gamma^2 \approx \rho(1 + |\mathbf{v}|^2/c^2)$  in equation (4), and we omit a thermal energy contribution proportional to  $\delta p$  ( $\sim \rho|\mathbf{v}|^2$ , by Bernoulli’s theorem), which we cannot calculate with our incompressible solver. Far from the source, we write  $h_{ij}^{\text{TT}} = h_+ e_{ij}^+ + h_\times e_{ij}^\times$ , with the polarizations defined by  $e_{yy}^+ = -e_{zz}^+ = e_{yz}^\times = e_{zy}^\times = 1$  for an observer on the  $x$ -axis.

In Figure 2a, we plot the  $h_+$  and  $h_\times$  polarizations versus time, as seen by an observer on the  $x$ -axis, for  $2 \leq m_a \leq 5$  (the signal is  $\sim 3$  times weaker on the  $z$ -axis, where the north-south asymmetry is not seen in projection). The amplitude is greatest for  $m_a = 5$  but depends weakly on  $m_a$ . Importantly,  $h_+$  and  $h_\times$  are  $\pi/2$  out of phase for all  $m_a$ , and we find  $|h_+| \ll |h_\times|$  for even  $m_a$ . These two signatures offer a promising target for future observations. The period ( $\approx 0.8\Omega_1^{-1}$ ) is similar for  $3 \leq m_a \leq 5$ , where a maximum of three helical vortices are excited (Li 2004) (we find that the torque at  $R_2$  oscillates with the same

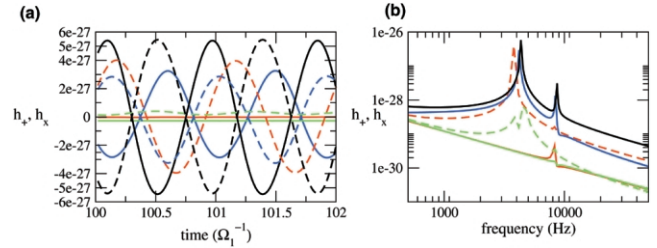


FIG. 2.—Gravitational waves from Taylor-Görtler vortices in a neutron star with  $\Omega_1/2\pi = 600$  Hz and  $r = 1$  kpc. (a) Signal  $h_{+,x}(t)$  and (b) frequency spectrum  $h_{+,x}(f)$ , for  $m_a = 2$  (red), 3 (blue), 4 (green), and 5 (black). Solid and dashed curves correspond to the plus and cross polarizations, respectively, as measured by an observer on the  $x$ -axis.

period). This too is good for detection, because several modes are likely to be excited in a real star. The period arises because the isosurface in Figure 1a forms a pattern with sixfold symmetry when projected onto the  $y$ - $z$  plane, with fundamental period  $4.4\Omega_1^{-1}$ .

In Figure 2b, we present the frequency spectra of the plus and cross polarizations. The two peaks, at  $f \approx 1.2\Omega_1$  and  $f \approx 2.4\Omega_1$ , have full widths at half-maximum of  $\sim 300$  Hz. This is caused by the subharmonics evident in Figure 1c, which arise because the northern and southern helical vortices start at unequal and variable longitudes. In addition, the peaks for even and odd  $m_a$  are displaced by  $\sim 500$  Hz, and the primary peak for  $m_a = 4$  is split. These two spectral signatures are a promising target for future observations. The even-odd displacement may arise because the phase speeds of the vortex patterns for  $m_a = 2$  and  $m_a = 3$  differ by  $\approx 0.01\Omega_1 R_1$  (Li 2004). For large  $f$ , we find  $h_{+,x}(f) \propto f^{-3/2}$ .

The squared signal-to-noise ratio can be calculated from  $(\text{S/N})^2 = 4 \int_0^\infty df |h(f)|^2 / S_h(f)$  (Creighton 2003), where we take  $S_h(f) = 10^{-50} [f/(0.6 \text{ kHz})]^2$  ( $0.2 \text{ kHz} \leq f \leq 3 \text{ kHz}$ ) for a  $10^8$  s integration with LIGO II, if the frequency and phase of the signal are known in advance (Brady et al. 1998). For a star with  $\Omega_1/2\pi = 600$  Hz, at  $r = 1$  kpc we find  $\text{S/N} = 0.21$  ( $m_a = 2$ ), 0.12 ( $m_a = 3$ ), 0.023 ( $m_a = 4$ ), and 0.22 ( $m_a = 5$ ), although there will be some leakage of signal when the coherent integration is performed, because the spectrum is not monochromatic. For  $m_a \leq 5$ , S/N increases (decreases) as  $m_a$  odd (even) increases. We also find  $\text{S/N} \propto \Omega_1^{7/2}$ , which implies that the fastest millisecond pulsars ( $\Omega_1/2\pi \sim 1$  kHz) and newly born pulsars with  $\Delta\Omega/\Omega_1 \sim 0.1$  are most likely to be detected. The flow states leading to turbulence at  $\text{Re} \geq 10^6$ , for example, shear waves, Stuart vortices, and “herringbone” waves (Nakabayashi & Tsuchida 1988), make contributions of similar order to the TGV signal in Figure 2.

The Reynolds number in the outer core of a neutron star,  $\text{Re} = 10^{10} [\rho/(10^{15} \text{ g cm}^{-3})]^{-1} [T/(10^8 \text{ K})]^2 [\Omega_*/(10^4 \text{ rad s}^{-1})]$  (Mastrano & Melatos 2005), where  $T$  is the temperature, typically exceeds the maximum Re in our simulations (due to computational capacity). For  $\text{Re} \geq 10^6$ , the flow is turbulent and therefore axisymmetric when time-averaged—but not instantaneously. In Kolmogorov turbulence, the characteristic flow speed in an eddy of wavenumber  $k$  scales as  $k^{-1/3}$ , the turbulent kinetic energy scales as  $k^{-5/3}$ , and the turnover time scales as  $k^{-2/3}$ . From equation (4), the rms wave strain scales as  $k^{-3/2} \int dk k^{-1/3}$  after averaging over Gaussian fluctuations, and it is dominated by the largest eddies (where most of the kinetic energy also resides). We therefore conclude that, even for  $\text{Re} \geq 10^6$ , the largest eddies, which resemble organized structures

like TGVs, dominate  $h_+$  and  $h_-$ , not the isotropic small eddies, but the signal is noisier. Hence, counterintuitively, we predict that hotter neutron stars (with lower Re) have narrower gravitational-wave spectra than cooler neutron stars, *ceteris paribus*.

We ignore compressibility when computing  $T_{00}$  ( $\delta p = 0$ ) and solving equation (1) numerically by pressure projection. Yet, realistically, neutron stars are strongly stratified (Abney & Epstein 1996), confining the meridional flow in Figure 1d into narrow layers near  $r = R_1$  and  $r = R_2$ . Stratification can be implemented crudely by using a low-pass spectral filter to artificially suppress  $v_r$  (Don 1994; Peralta et al. 2006). We postpone this to future work.

We acknowledge the computer time supplied by the Australian Partnership for Advanced Computation (APAC) and the Victorian Partnership for Advanced Computation (VPAC). We thank Professor Li Yuan, from the Chinese Academy of Sciences, for very helpful discussions. We also thank Professor S. Balachandar, from the University of Illinois at Urbana-Champaign, for supplying us with his original Navier-Stokes pseudospectral solver, from which our spherical Couette solver was developed.

## REFERENCES

- Abney, M., & Epstein, R. I. 1996, *J. Fluid Mech.*, 312, 327  
 Alpar, M. A. 1978, *J. Low Temp. Phys.*, 31, 803  
 Andersson, N. 1998, *ApJ*, 502, 708  
 ———. 2003, *Classical Quantum Gravity*, 20, R105  
 Andersson, N., Kokkotas, K., & Schutz, B. F. 1999, *ApJ*, 510, 846  
 Bagchi, B., & Balachandar, S. 2002, *J. Fluid. Mech.*, 466, 365  
 Barenghi, C. F., Samuels, D. C., Bauer, G. H., & Donnelly, R. J. 1997, *Phys. Fluids*, 9, 2631  
 Baym, G., Epstein, R. I., & Link, B. 1992, *Physica B*, 178, 1  
 Brady, P. R., Creighton, T., Cutler, C., & Schutz, B. F. 1998, *Phys. Rev. D*, 57, 2101  
 Canuto, C., Hussaini, M., Quarteroni, A., & Zang, T. 1988, *Spectral Methods in Fluid Dynamics* (Berlin: Springer)  
 Chong, M. S., Perry, A. E., & Cantwell, B. J. 1990, *Phys. Fluids A*, 2, 765  
 Comer, G. L. 2002, *Found. Phys.*, 32, 1903  
 Creighton, T. 2003, *Classical Quantum Gravity*, 20, S853  
 Dimmelmeier, H., Font, J. A., & Müller, E. 2002, *A&A*, 393, 523  
 Don, W. S. 1994, *J. Comput. Phys.*, 110, 103  
 Fujimoto, M. Y. 1993, *ApJ*, 419, 768  
 Giacobello, M. 2005, Ph.D. thesis, Univ. Melbourne  
 Hall, H. E., & Vinen, W. F. 1956, *Proc. R. Soc. London A*, 238, 204  
 Henderson, K. L., & Barenghi, C. F. 2004, *Theor. Comput. Fluid Dyn.*, 18, 183  
 Jeong, J., & Hussain, F. 1995, *J. Fluid Mech.*, 285, 69  
 Jones, P. B. 1998, *MNRAS*, 296, 217  
 Junk, M., & Egbers, C. 2000, in *Lecture Notes in Physics*, 549, *Physics of Rotating Fluids*, ed. C. Egbers & G. Pfister (Berlin: Springer), 215  
 Levin, Y., & D'Angelo, C. 2004, *ApJ*, 613, 1157  
 Levin, Y., & Ushomirsky, G. 2001, *MNRAS*, 324, 917  
 Li, Y. 2004, *Sci. China A*, 47(S1), 81  
 Link, B. 2003, *Phys. Rev. Lett.*, 91, 101101  
 Lyne, A. G., Shemar, S. L., & Smith, F. G. 2000, *MNRAS*, 315, 534  
 Marcus, P. S., & Tuckerman, L. S. 1987a, *J. Fluid Mech.*, 185, 1  
 ———. 1987b, *J. Fluid Mech.*, 185, 31  
 Mastrano, A., & Melatos, A. 2005, *MNRAS*, 361, 927  
 Misner, C. W., Thorne, K. S., & Wheeler, J. A. 1973, *Gravitation* (San Francisco: Freeman)  
 Nakabayashi, K. 1983, *J. Fluid Mech.*, 132, 209  
 Nakabayashi, K., & Tsuchida, Y. 1988, *J. Fluid Mech.*, 194, 101  
 ———. 1995, *J. Fluid Mech.*, 295, 43  
 ———. 2005, *Phys. Fluids*, 17(10), No. 4110  
 Ott, C. D., Burrows, A., Livne, E., & Walder, R. 2004, *ApJ*, 600, 834  
 Peralta, C., Melatos, A., Giacobello, M., & Ooi, A. 2005, *ApJ*, 635, 1224  
 ———. 2006, *ApJ*, submitted  
 Prix, R., Comer, G. L., & Andersson, N. 2004, *MNRAS*, 348, 625  
 Reisenegger, A. 1993, *J. Low Temp. Phys.*, 92, 77  
 Rezzolla, L., Lamb, F. K., & Shapiro, S. L. 2000, *ApJ*, 531, L139  
 Ruderman, M. 1991, *ApJ*, 382, 587  
 Sedrakian, A., & Cordes, J. M. 1999, *MNRAS*, 307, 365  
 Sedrakian, A. D., & Sedrakian, D. M. 1995, *ApJ*, 447, 305  
 Sha, W., & Nakabayashi, K. 2001, *J. Fluid Mech.*, 431, 323  
 Shemar, S. L., & Lyne, A. G. 1996, *MNRAS*, 282, 677  
 Shibata, M., & Uryū, K. 2000, *Phys. Rev. D*, 61, 064001  
 Wilde, P. D., & Vanyo, J. P. 1995, *Phys. Earth Planet. Inter.*, 91, 31  
 Wulf, P., Egbers, C., & Rath, H. J. 1999, *Phys. Fluids*, 11, 1359  
 Yakovlev, D. G., Levenfish, K. P., & Shibano, Y. A. 1999, *Phys.-Uspekhi*, 42, 737  
 Yavorskaya, I. M., Belayev, Yu. N., & Monakhov, A. A. 1975, *Soviet Phys.-Dokl.*, 20, 209  
 ———. 1977, *Soviet Phys.-Dokl.*, 22, 717  
 Zikanov, O. Yu. 1996, *J. Fluid Mech.*, 310, 293